Article

Unraveling the Durable Water Oxidation Mechanism of Multi-principal Elemental Metal Catalyst

QIAN Fangren[1,2,3], WAN Jiaqi[2], JIANG Wei[3], LI Rongyao[3], YI Luocai[1,2], CHEN Shuangming[3], CHEN Qingjun[1,2]✉ and SONG Li[3]✉

Received January 15, 2025
Accepted February 15, 2025

Nanoscale multi-principal element metal (MPEM) offers a diverse and adjustable compositional range of active, holding promise for applications in water oxidation. Nevertheless, the synthesis of MPEM nanoparticles poses challenges owing to the tendency of particles to experience growth, aggregation, or phase separation during annealing processes. Here, we introduce a rapid heating and cooling method that enables the fabrication of rare earth-containing MPEM through instantaneous heating and rapid cooling processes. The TEM results indicate that the metal particles are roughly around 120 nm in size, with uniform distribution of various metal elements on the particles. The X-ray characterizations further reveal that the metal catalyst exhibits predominantly a face-centered cubic (FCC) structure with partial oxidation on the surface. Notably, the obtained MPEM catalysts exhibit a current density of 10 mA/cm^2 with an overpotential of 244 mV, which is 26 and 104 mV lower than the overpotentials of FeCoNiCr and commercial RuO_2. Moreover, the MPEM catalyst can operate stably for over 200 h at current densities of 10 and 100 mA/cm^2.

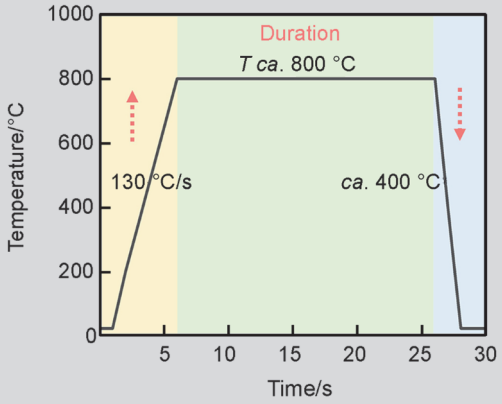

Keywords Joule heating; Multi-principal element particle; Oxygen evolution reaction

1 Introduction

Hydrogen energy is both clean and renewable, offering a promising alternative to fossil fuels.[1−3] Clean hydrogen energy can be generated through electrocatalytic water splitting.[4−6] During electrocatalytic water splitting, the anodic oxygen evolution reaction (OER) encompasses a gradual four-electron transfer mechanism, impeding the overall efficiency of hydrogen production.[7−10] Therefore, the development of efficient OER catalysts to enhance reaction kinetics is crucial for large-scale hydrogen production.[11−14]

Multi-principal elemental metal (MPEM) catalyst exhibit exceptional catalytic efficiency and durability due to their intricate composition, entropy effects, and homogeneous element distribution.[15−17] The increased configurational entropy resulting from blending diverse elements in similar proportions stabilizes the solid solutions and improves their resistance to corrosion.[18] Moreover, lattice distortions originating from varying atomic sizes bring about significant changes in the electronic structure of these alloys. MPEM catalysts present a multitude of opportunities for altering structural, electronic, and catalytic properties. The design of MPEM represents a potent approach for enhancing active sites and electronic configurations, leading to remarkable OER catalytic performance and stability.[19] However, numerous metallic elements demonstrate extensive miscibility gaps within their phase diagrams owing to the positive enthalpy of mixing. As a result, the fabrication of MPEM catalysts often confronts issues of segregation or coarsening when employing conventional techniques like prolonged thermal annealing, co-reduction, and galvanic replacement. The synthesis of MPEM nanoparticles, involving more than three elements, necessitates precise control over reaction conditions, a task that has proven challenging with traditional synthesis methods like furnace annealing due to slow heating and cooling rates.[20] Notably, the extended heating periods characteristic of annealing procedures leads to particle

✉ SONG Li
song2012@ustc.edu.cn
✉ CHEN Qingjun
qjchen@gia.cas.cn
1. School of Rare Earths, University of Science and Technology of China, Hefei 230026, P. R. China;
2. Key Laboratory of Rare Earths, Ganjiang Innovation Academy, Chinese Academy of Sciences, Ganzhou 341000, P. R. China;
3. National Synchrotron Radiation Laboratory, University of Science and Technology of China, Hefei 230029, P. R. China

https://doi.org/10.1007/s40242-025-5010-3

growth and aggregation, impeding the creation of nanoscale MPEM. Furthermore, the thermodynamic immiscibility of the component elements poses an additional challenge, often resulting in phase separation.[21]

In this study, we illustrate the fabrication of nanoscale MPEM particles measuring 120 nm in diameter, incorporating up to five different elements. Remarkably, we achieve this without experiencing particle growth or phase separation through the implementation of a distinctive rapid Joule heating strategy.[22,23] By utilizing MPEM as electrocatalysts for the OER process, we achieved low overpotentials of 244 and 449 mV at current densities of 10 and 500 mA/cm^2, respectively. Remarkably, the electrocatalysts demonstrated durability for more than 200 h at 10 and 100 mA/cm^2 without notable performance degradation. The rapid Joule-heating preparation approach and the evaluation of OER performance with the MPEM lay a solid groundwork for the advancement of OER catalysts.

2 Experimental

2.1 Catalyst Preparation

The synthesis of FeCoNiCrSm nanoparticles commenced with the dissolution of 0.2 mmol of individual metal salts [$Fe(NO_3)_3·9H_2O$, $Co(NO_3)_2·6H_2O$, $Ni(NO_3)_2·6H_2O$, $Cr(NO_3)_3·9H_2O$, and $Sm(NO_3)_3·6H_2O$] in 200 mL of ethanol *via* sonication for a minimum duration of 30 min to generate the mixed precursor solution. Subsequently, 200 mg of commercial carbon (Ketjen black, ECP-600) was introduced into the precursor solution. The resulting mixture was agitated at 80 °C until reaching a desiccated state. The precursor/carbon powders were then dispersed onto two carbon paper channels and linked to two copper electrodes employing a Joule heating apparatus (Hefei *In-situ* Technology Co., Ltd., CIS-JH3.3-P) situated within an argon-filled glovebox. The parameters of the electrical pulse, encompassing current (temperature) and duration (thermal shock time), were modifiable. Analogous procedures were implemented for the synthesis of alternative alloys, with the exception of particular metal salts.

2.2 Preparation of Catalyst Ink

For the preparation of the working electrode, 5 mg of the synthesized catalysts and commercial RuO_2 (99.99%, Shanghai McLean Biochemical Technology Co., Ltd.) were combined with 950 μL of ethanol and 50 μL of Nafion (5%, mass fraction) and sonicated for 2 h to produce a homogeneously mixed catalyst ink solution. Following this, the prepared ink was applied onto the carbon paper electrode with a tailored loading capacity specific to the catalysts being studied.

2.3 Materials Characterization

X-Ray diffraction (XRD) patterns of the samples were collected by a Smart Lab 9 kW X-ray diffractometer within the 2θ range of 10°—80°. Transmission electron microscopy (TEM) and high-angle annular dark-field scanning transmission electron microscopy (HAADF-STEM) images were taken with a JEOL-2100F transmission electron microscope operating at 200 kV. The samples were subjected to analysis through inductively coupled plasma optical emission spectroscopy (ICP-OES) by the ICPE9000 instrument.

X-Ray absorption near-edge structure (XANES) and extended X-ray absorption fine structure (EXAFS) data for Co, Ni and Cr were collected in fluorescence mode at the X-ray absorption spectroscopy beamline of the Shanghai Synchrotron Radiation Facility, China (operating at 200 mA, 3.0 GeV).

2.4 Electrochemical Testing

The experiments of the OER performance were conducted employing a traditional three-electrode cell setup in a 1.0 mol/L KOH solution. The catalyst ink was applied onto a carbon paper as the working electrode in the OER measurements.

For the formulation of the catalyst ink, 5 mg of the catalyst was added to a solution comprising 0.95 mL of ethanol and 0.05 mL of a 5% (mass fraction) Nafion, and then uninterrupted ultrasonication for roughly 60 min. Subsequently, the prepared ink was applied to the working electrode. All potentials were standardized to the reversible hydrogen electrode (RHE) utilizing the formula: $E_{RHE}=E_{Hg/HgO}+0.059\times pH+0.098$. Linear sweep voltammetry (LSV) curves were obtained over the potential range from 0.8 V to 1.8 V *versus* RHE with a scan rate of 5 mV/s to evaluate the OER performance of catalysts. The overpotential (η) of OER was determined using the formula: $\eta=E_{RHE}-1.23$ V.

For the examination of reaction kinetics, the Tafel slope was determined by utilizing the equation: $\eta=b\lg j+a$, where b represents the Tafel slope and j denotes the current density. Furthermore, electrochemical impedance spectroscopy (EIS) was conducted within a frequency range from 0.1 Hz 10^6 Hz at 1.55 V *versus* RHE. Cyclic voltammetry (CV) in the non-Faradaic range at scan rates of 5, 10, 15, 20, 25, 30, and 35 mV/s was utilized to ascertain the electrochemical double-layer capacitances of the catalysts. The double-layer capacitance (C_{dl}) value of the catalyst was determined by analyzing the slope of the plot depicting

https://doi.org/10.1007/s40242-025-5010-3

current density *versus* scan rate. Assuming 40 μF/cm² as a typical specific capacitance value for a flat surface, the electrochemical surface area (ECSA) of the samples was conducted using the equation: $ECSA=C_{dl}/40\ \mu F\cdot cm^{-2}$ per cm^2_{ECSA}.

3 Results and Discussion

3.1 Preparation and Structure of MPEM

The preparation procedure of FeCoNiCrSm catalyst by the Joule-heating technique is elucidated in Fig. 1, A_1—A_3. The equably mixed solution, consisting of different metal salts and carbon powder was dissolved in ethanol in equimolar proportions to guarantee composition of samples (Fig. $1A_1$). Subsequently, the resultant solution was vigorously stirred at 80 °C, promoting solvent evaporation and culminating in the generation of precursor powder. The combined powder underwent rapid high-temperature heating. By means of the rapid heating process, the amalgamated salts underwent decomposition and reduction under commercial carbon, culminating in the formation of FeCoNiCrSm. The FeCoNiCr nanoparticles were synthesized using the same method, except without Sm. The heating procedure is depicted in Fig. $1A_2$, highlighting the rapid heating and cooling rates attained through Joule heating. The structural of FeCoNiCrSm is depicted in Fig. $1A_3$. Transmission electron microscopy (TEM) image reveals FeCoNiCrSm as spherical particles measuring around 120 nm, with the exposed edges improving the accessibility of active sites and enhancing the OER performance (Fig. 1, B and C). The atomic model of FeCoNiCrSm sample was unveiled through aberration-corrected scanning transmission electron microscopy (AC-STEM) (Fig. 1D). The atomic configurations within FeCoNiCrSm sample were discerned by the obvious atomic columns. XRD patterns of FeCoNiCrSm and FeCoNiCr are illustrated in Fig. 1E, where both FeCoNiCrSm and FeCoNiCr demonstrate a pronounced face-centered cubic (FCC) crystal phase with obvious diffraction peaks vested in the (111), (200), and (220) surfaces, in alignment with TEM findings. EDS mappings (Fig. 1F) exhibit the uniform dispersion of Fe, Co, Ni, Cr, and Sm metals in a single particle without eliguation. Fig. S1 in the Electronic Supplementary Information, ESI also exhibits the uniform dispersion of Fe, Co, Ni and Cr metals in a single particle without eliguation for FeCoNiCr catalyst. The findings from XRD and STEM-mapping both indicate that through a thermal shock method, all metal elements are uniformly distributed on the particles of the catalyst, demonstrating the successful preparation of MPEM catalysts.

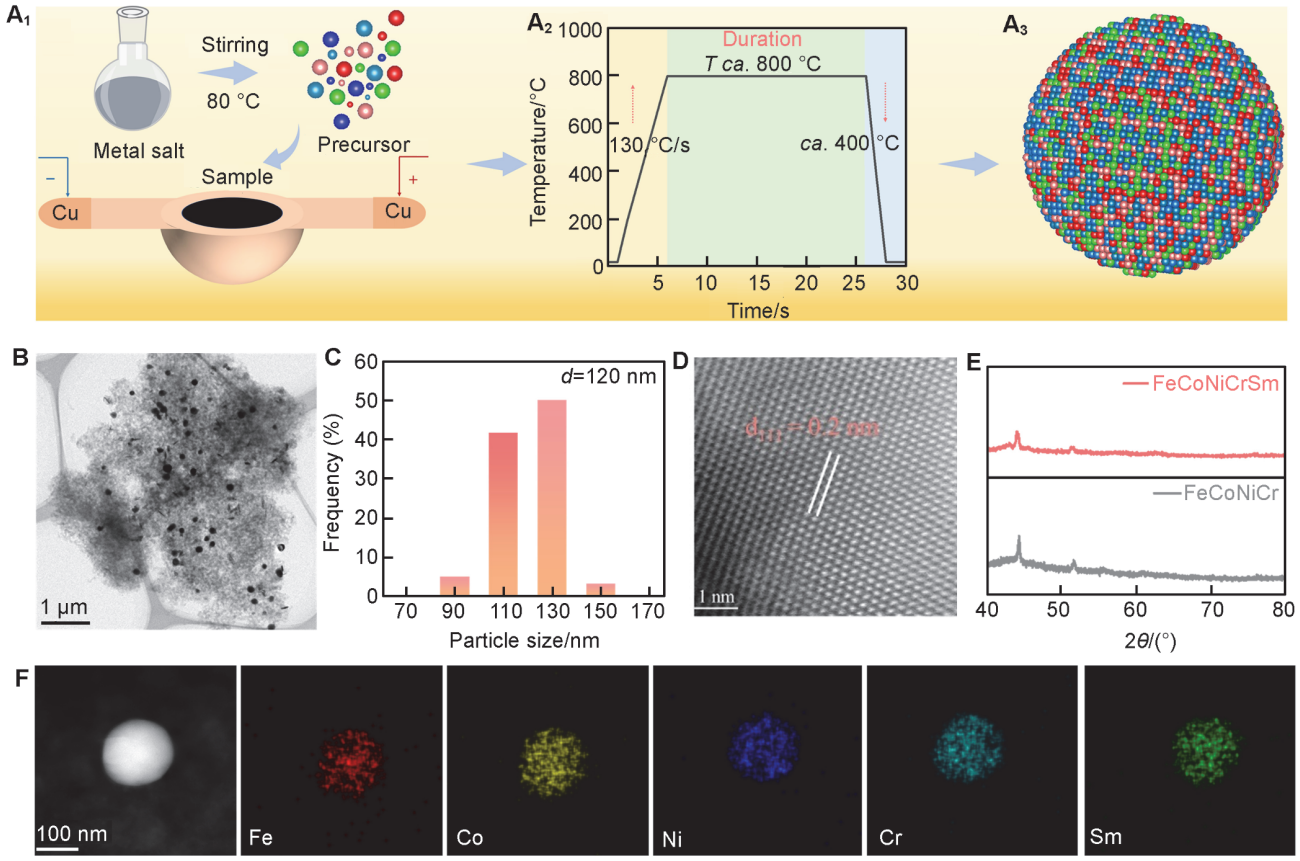

Fig. 1 Structures of the obtained materials

(A) Schematic diagram illustrating the synthesis of FeCoNiCrSm using rapid Joule heating; (B) a representative TEM image; (C) the diameter distribution of FeCoNiCrSm; (D) HAADF-STEM image of FeCoNiCrSm; (E) X-ray diffraction spectra of prepared samples; (F) EDS elemental mappings.

https://doi.org/10.1007/s40242-025-5010-3

X-Ray absorption spectroscopy (XAS) was performed to analyze the chemical states and local coordination environment.[24,25] The oxidation states of Co, Ni, and Cr atoms in FeCoNiCrSm were initially evaluated through K-edge X-ray absorption near edge spectroscopy (XANES). The XANES spectra indicate that the absorption energies of Co, Ni, and Cr in FeCoNiCrSm lie between the metal foil and the oxide, suggesting the oxidation state of the metals is found to be between the metallic and oxidized states, indicating partial oxidation of the metals on the surface of the FeCoNiCrSm catalyst, which is more favorable for the OER process (Fig. 2, A—C and Fig. S2 in the ESI). Fourier-transformed (FT) $k3$-weighted $\chi(k)$-function Co, Ni, and Cr K-edge extended X-ray absorption fine structure (EXAFS) analyses provided detailed insights into the structures of Co, Ni, and Cr sites in FeCoNiCrSm configurations. The EXAFS patterns of Co, Ni, and Cr at the K-edge are depicted in Fig. 2, D—F and juxtaposed with the corresponding standard metal foil and oxide references. The broad peak around 2 Å (1 Å=0.1 nm) (Co and Ni) is attributed to the coexistence of metal-oxygen bonds and metal-metal bond. (without phase correction). The EXAFS of Cr is attributed to the Cr—O (1.6 Å) bond and Cr—Cr bond (2.6 Å), and this discovery indicates a clear oxidation of Cr on the surface of the catalyst, leading to a transition to an oxidized state. The results of XAS indicate that the surfaces of MPEM catalyst have undergone varying degrees of oxidation, with Cr exhibiting the most pronounced oxidation, thus highlighting the oxygen affinity of Cr. Due to the OER occurring at oxidizing potentials, under alkaline conditions, most metal or metal oxide catalysts will reconstruct into M-OOH catalysts during the reaction process. The true active centers are also provided by M-OOH.[4,5] Therefore, weak oxidation on the surface of MPEM catalysts will not affect OER performance and may even promote the OER process.

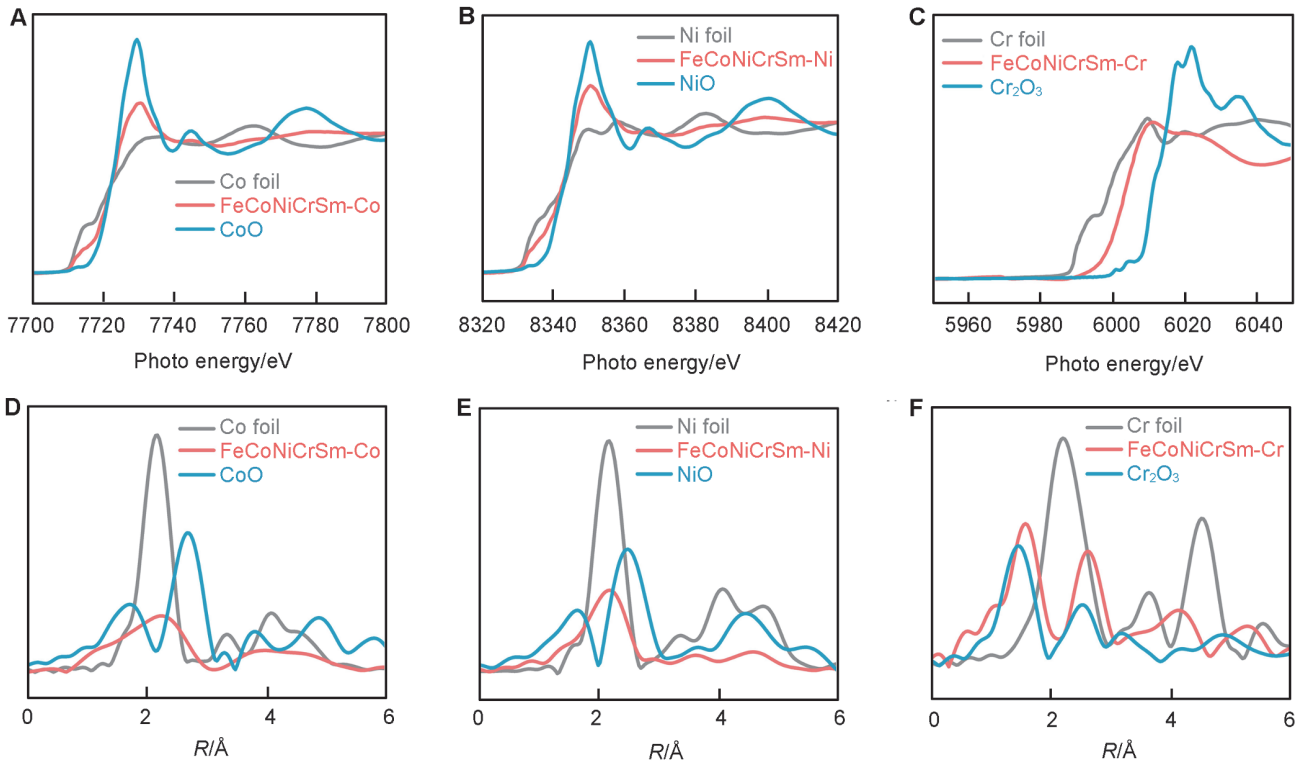

Fig. 2 Examination of the local struture of FeCoNiCrSm
(A—C) XANES spectra at the Co, Ni, and Cr K-edges; (D—F) Fourier-transformed K-edge EXAFS spectra of Co, Ni, and Cr within the FeCoNiCrSm system, respectively. Reference samples included metal foils and oxides.

3.2 OER Performance

The electrocatalytic performance of the synthesized materials was assessed in relation to the commercial benchmark RuO_2 using OER tests. The experiments were carried out in a 1.0 mol/L potassium hydroxide (KOH), where the potentials were calibrated with respect to the RHE standard.[26,27] Linear sweep voltammetry (LSV) of different catalysts is depicted in Fig. 3A, and the LSV plots for the FeCoNiCrSm catalysts demonstrated enhanced efficacy, necessitating a mere overpotential of 244 mV at 10 mA/cm^2, outperforming those of FeCoNiCr (270 mV) and the commercial RuO_2 (348 mV). Notably, the as-synthesized FeCoNiCrSm material demonstrated an exceptional overpotential of 449 mV at a current density of 500 mA/cm^2, outperforming previous studies. The Tafel slope of

https://doi.org/10.1007/s40242-025-5010-3

FeCoNiCrSm (116.8 mV/dec) exceeds those of FeCoNiCr (131.9 mV/dec) and the commercial RuO_2 (147.5 mV/dec) (Fig. 3B), suggesting improved reaction activity of the FeCoNiCrSm material during the OER. EIS patterns (Fig. 3C) show the smallest charge transfer resistance (R_{ct}) of 6.69 Ω for FeCoNiCrSm among all materials, indicating improved charge transport and enhanced OER kinetics. The ECSA of the prepared samples demonstrates a strong correlation with the C_{dl}, as indicated by the CV plots at different scan rates (Fig. S3 in the ESI). The elevated C_{dl} value of FeCoNiCrSm (48.5 mF) in contrast to that of FeCoNiCr (14.2 mF) attributed to its smaller particle diameter (Fig. S4 in the ESI). The overpotential at 10 mA/cm², represented as η_{10}, the Tafel slope, ECSA, EIS, and the current density at 1.6 V of the fabricated catalysts are additionally juxtaposed in Fig. 3D, corroborating the superior OER performance of the MPEM catalyst. After the introduction of Sm, there has been a significant enhancement in the catalytic performance, indicating that Sm plays a crucial role in MPEM catalysts. Lanthanide (Ln) elements, characterized by the shielding of the 4*f* orbital by the 5*s* and 5*p* orbitals, have the capacity to diminish external influences, enabling accurate and continual adjustment of catalysts for enduring OER electrocatalysis. The inclusion of Ln elements provides a versatile method for finely tuning and enhancing the electrocatalytic capabilities of catalysts. This is facilitated by the shielding influence of the 5*s*/5*p* orbitals, the distinctive electron configuration of the 4*f* orbital, a range of electronic energy levels, and the capacity to accommodate diverse coordination numbers.[28] Therefore, the introduction of Sm has enhanced the OER activity of the MPEM catalyst. Long-term durability stands as a critical parameter for assessing OER catalysts, and the endurance of the FeCoNiCrSm catalyst was evaluated under different current density. Fig. 3E illustrates the potential exhibits minimal variation over extended periods of 200 h at 10 and 100 mA/cm², demonstrating the impressive durability of FeCoNiCrSm.

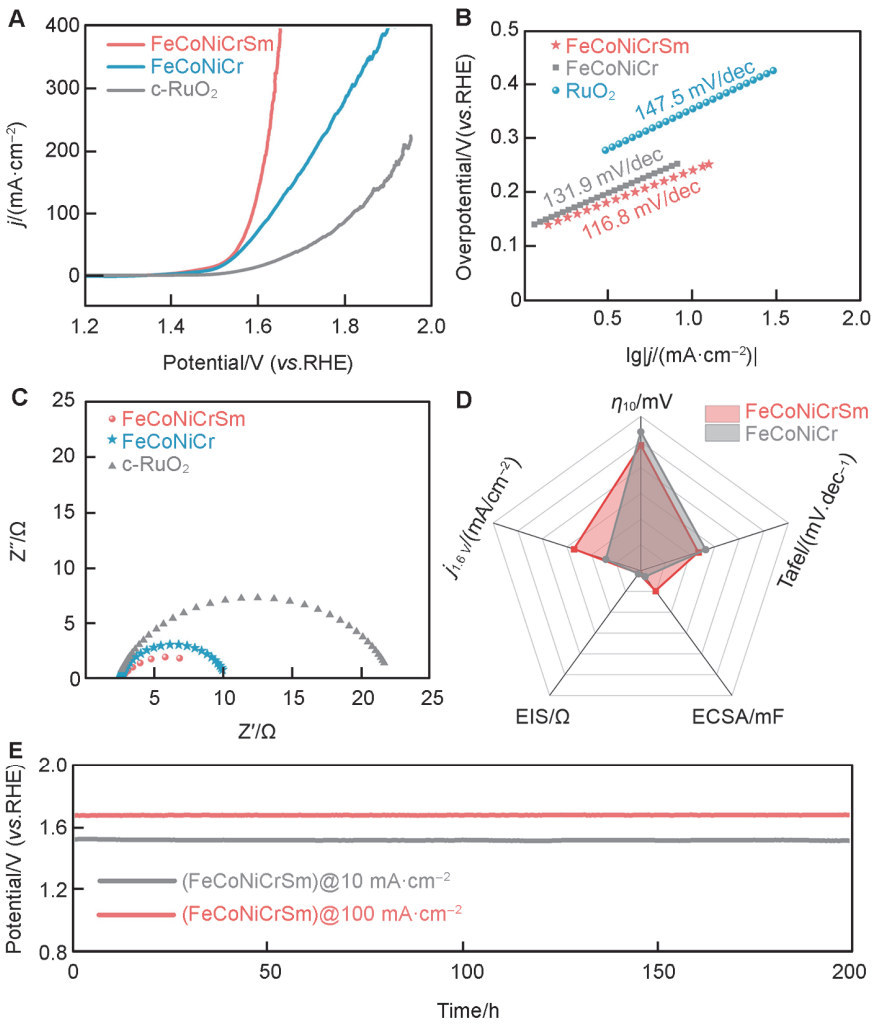

Fig. 3 Electrocatalytic oxygen evolution reaction (OER) performance assessment of catalysts

(A) LSV curves for FeCoNiCrSm, FeCoNiCr, and commercial RuO_2; (B) Tafel plots extrapolated from the LSV curves in (A); (C) EIS Nyquist plots for FeCoNiCrSm, FeCoNiCr, and commercial RuO_2; (D) radar diagram illustrating key OER performance metrics for FeCoNiCrSm, FeCoNiCr, and commercial RuO_2; (E) chronopotentiometry curves for FeCoNiCrSm at fixed current densities of 10 and 100 mA/cm².

3.3 Exploration of OER Durability

The FeCoNiCrSm post-stability experiments were scrutinized to obtain a thorough comprehension of the mechanisms underpinning its enduring durability. Fig. 4 depicts the TEM images of FeCoNiCrSm post the prolonged stability assessmen, the original morphology and lattice structure were well maintained, with all metal constituents uniformly distributed within the FeCoNiCrSm nanoparticles. This observation offers further substantiation of the robust stabilization of FeCoNiCrSm during the OER progression. The MPEM catalysts exhibit exceptional structural stability and tunable catalytic activity when utilized as catalysts due to the mixed effects of multiple elements, lattice distortion effects in structure, sluggish diffusion effects in kinetics, and the "cocktail" effect in properties.[27,29]

https://doi.org/10.1007/s40242-025-5010-3

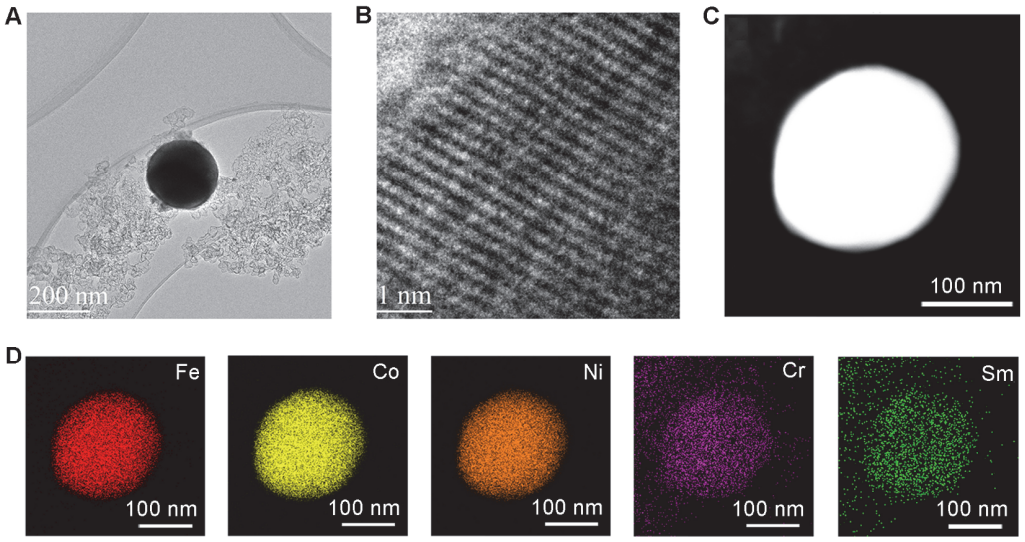

Fig. 4 Exploration of the OER durability mechanism of FeCoNiCrSm
(A—C) TEM images; (D) TEM-EDS mappings of FeCoNiCrSm post-stability test.

4 Conclusions

In conclusion, we have effectively incorporated multiple elemental metals into the lattice, culminating in the creation of a cohesive solid-solution structure known as MPEM. The transition from different metal configurations to a singular-phase MPEM was all verified through various characterization methodologies. The MPEM anode catalyst achieved 0.5 A/cm^2 at 449 mV overpotential and exhibited significant stability during electrolysis over 200 h at 0.1 A/cm^2. The characterizations before and after cycling suggest that the morphology and lattice of the catalyst have not undergone significant changes, providing a robust structural foundation for the stability of the catalyst. This perspective of strategically manipulating multi-principal elemental metal in catalysts presents a promising method for developing and producing durable OER materials.

Electronic Supplementary Information

Supplementary material is available in the online version of this article at http://dx.doi.org/10.1007/s40242-025-5010-3.

Acknowledgements

This work was supported by the National Key Research and Development Program of China (No. 2022YFA1504100), the National Natural Science Foundation of China (Nos. 92061125, 12225508, 12322515, 22075264, 22309184), the Strategic Priority Research Program of the Chinese Academy of Sciences (No. XDA0410401), the Youth Innovation Promotion Association of CAS (No. 2022457), the Jiangxi Natural Science Foundation, China (No. 20212ACB213009), and the Fundamental Research Funds for the Central Universities, China (No. WK2060000039).
We acknowledge the Shanghai Synchrotron Radiation Facility, China (BL14W1) and the Beijing Synchrotron Radiation Facility, China (1W1B) for the material characterization of synchrotron X-ray absorption spectrum.

Conflicts of Interest

The authors declare no conflicts of interest.

References

[1] Gunathilake C., Soliman I., Panthi D., Tandler P., Fatani O., Ghulamullah N. A., Marasinghe D., Farhath M., Madhujith T., Conrad K., Du Y., Jaroniec M., *Chem. Soc. Rev.*, **2024**, *53*, 10900.
[2] Liu R. T., Xu Z. L., Li F. M., Chen F. Y., Yu J. Y., Yan Y., Chen Y., Xia B. Y., *Chem. Soc. Rev.*, **2023**, *52*, 5652.
[3] Wang Y., Wang M., Yang Y., Kong D., Meng C., Zhang D., Hu H., Wu M., *Chem. Catalysis.*, **2023**, *3*, 100643.
[4] Mei Y., Chen J., Wang Q., Guo Y., Liu H., Shi W., Lin C., Yuan Y., Wang Y., Xia B. Y., Yao Y., *Science Advance*, **2024**, *10*, eadq6758.
[5] Qian Z. X., Liang G. H., Shen L. F., Zhang G., Zheng S., Tian J. H., Li J. F., Zhang H., *J. Am. Chem. Soc.*, **2024**, *147*, 1334.
[6] Huang Y., Wang Z., Xiao H., Liu Q., Wang X., *J. Am. Chem. Soc.*, **2024**, *146*, 29006.
[7] Huang Z.-F., Song J., Du Y., Xi S., Dou S., Nsanzimana J. M. V., Wang C., Xu Z. J., Wang X., *Nature Energy*, **2019**, *4*, 329.
[8] Xu S., Feng S., Yu Y., Xue D., Liu M., Wang C., Zhao K., Xu B., Zhang J. N., *Nat. Commun.*, **2024**, *15*, 1720.
[9] Abdelhafiz A., Wang B., Harutyunyan A. R., Li J., *Advanced Energy Materials*, **2022**, *12*, 220074.
[10] Wu H., Lu Q., Li Y., Wang J., Li Y., Jiang R., Zhang J., Zheng X., Han X., Zhao N., Li J., Deng Y., Hu W., *Nano Lett.*, **2022**, *22*, 6492.
[11] Hu Y., Zheng Y., Jin J., Wang Y., Peng Y., Yin J., Shen W., Hou Y., Zhu L., An L., Lu M., Xi P., Yan C. H. *Nat. Commun.*, **2023**, *14*, 1949.
[12] Pei Z., Zhang H., Wu Z.-P., Lu X. F., Luan D., Lou X. W., *Science Advance*, **2023**, *9*, eadh1320.
[13] Li Y., Zhao G., Zuo S., Wen L., Liu Q., Zou C., Ren Y., Kobayashi Y., Tao H., Luan D., Huang K., Cavallo L., Zhang H., *Adv. Mater.*, **2024**, e2407386.
[14] Zuo S., Wu Z. P., Xu D., Ahmad R., Zheng L., Zhang J., Zhao L., Huang W., Al Qahtani H., Han Y., Cavallo L., Zhang H., *Nat. Commun.*, **2024**, *15*, 9514.
[15] Cui M., Yang C., Hwang S., Yang M., Overa S., Dong Q., Yao Y., Brozena A. H., Cullen D. A., Chi M., Blum T. F., Morris D., Finfrock Z., Wang X., Zhang P., Goncharov V. G., Guo X., Luo J., Mo Y., Jiao F., Hu L., *Science Advance*, **2022**, *8*, eabm4322.
[16] Yao Y., Huang Z., Xie P., Lacey S. D., Jacob R. J., Xie H., Chen F.,

Nie A., Pu T., Rehwoldt M., Yu D., Zachariah M. R., Wang C., Shahbazian-Yassar R., Li J., Hu L., *Science*, **2018**, *359*, 1489.

[17] Yao Y., Dong Q., Brozena A., Luo J., Miao J., Chi M., Wang C., Kevrekidis I. G., Ren Z. J., Greeley J., Wang G., Anapolsky A., Hu L., *Science*, **2022**, *376*, eabn3103.

[18] Huang Z., Li T., Li B., Dong Q., Smith J., Li S., Xu L., Wang G., Chi M., Hu L., *Journal of the American Chemical Society*, **2024**, *146*, 2167.

[19] Qiao H., Saray M. T., Wang X., Xu S., Chen G., Huang Z., Chen C., Zhong G., Dong Q., Hong M., Xie H., Shahbazian-Yassar R., Hu L., *ACS Nano,* **2021**, *15*, 14928.

[20] Yao Y., Huang Z., Hughes L. A., Gao J., Li T., Morris D., Zeltmann S. E., Savitzky B. H., Ophus C., Finfrock Y. Z., Dong Q., Jiao M., Mao Y., Chi M., Zhang P., Li J., Minor A. M., Shahbazian-Yassar R., Hu L., *Matter,* **2021**, *4*, 2340.

[21] Li T., Yao Y., Huang Z., Xie P., Liu Z., Yang M., Gao J., Zeng K., Brozena A. H., Pastel G., Jiao M., Dong Q., Dai J., Li S., Zong H., Chi M., Luo J., Mo Y., Wang G., Wang C., Shahbazian-Yassar R., Hu L., *Nature Catalysis,* **2021**, *4*, 62.

[22] Shen P., Zhao J., Gao Y., Lin Y., Han Y., Xu K., *Science China Chemistry,* **2024**, *67*, 1976.

[23] Lin Y., Geng B., Zheng R., Chen W., Zhao J., Liu H., Qi Z., Yu Z., Xu K., Liu X., Yang L., Shan L., Song L., *Nat. Commun.,* **2025**, *16*, 286.

[24] Hao J., Zhuang Z., Cao K., Gao G., Wang C., Lai F., Lu S., Ma P., Dong W., Liu T., Du M., Zhu H., *Nat. Commun.,* **2022**, *13*, 2662.

[25] Feng G., Ning F., Song J., Shang H., Zhang K., Ding Z., Gao P., Chu W., Xia D., *J. Am. Chem. Soc.,* **2021**, *143*, 17117.

[26] Liu Y.-H., Hsieh C.-J., Hsu L.-C., Lin K.-H., Hsiao Y.-C., Chi C.-C., Lin J.-T., Chang C.-W., Lin S.-C., Wu C.-Y., Gao J.-Q., Pao C.-W., Chang Y.-M., Lu M.-Y., Zhou S., Yang T.-H., *Science Advance,* **2023**, *9*, eadf9931.

[27] Zhu H., Sun S., Hao J., Zhuang Z., Zhang S., Wang T., Kang Q., Lu S., Wang X., Lai F., Liu T., Gao G., Du M., Wang D., *Science,* **2023**, *16*, 619.

[28] Li L., Zhang G., Zhou C., Lv F., Tan Y., Han Y., Luo H., Wang D., Liu Y., Shang C., Zeng L., Huang Q., Zeng R., Ye N., Luo M., Guo S., *Nat. Commun.,* **2024**, *15*, 4974.

[29] Cao G., Liang J., Guo Z., Yang K., Wang G., Wang H., Wan X., Li Z., Bai Y., Zhang Y., Liu J., Feng Y., Zheng Z., Lu C., He G., Xiong Z., Liu Z., Chen S., Guo Y., Zeng M., Lin J., Fu L., *Nature,* **2023**, *619*, 73.

https://doi.org/10.1007/s40242-025-5010-3